The secondary Bjerknes force between two oscillating bubbles in Kelvin-Voigt-type viscoelastic fluids driven by harmonic ultrasonic pressure

Haiyan Chen, Zhenmin Lai, Ziliang Chen

School of Material and Energy, Guangdong University of Technology, Guangzhou, China, 510006

Yi Li*

School of Mathematics and Statistics, University of Sheffield, Sheffield, UK, S3 7RH

Abstract

The interaction between two small bubbles experiencing transient cavitation in a nonlinear Kelvin-Voigt fluid is investigated. The time-delay effect in the interaction is incorporated in the coupled Keller-Miksis model. The refined model predicts that bubbles with radii smaller than 2μm will be repelled by large bubbles, in contrast to predictions from previous models. The matching pressure needed to obtain same level of transient cavitation in different Kelvin-Voigt fluids is shown to depend mainly on the shear modulus and is insensitive to other parameters, which makes it a useful parameter to correlate the results. When the radii of the bubbles fall between 4μm and 6μm, the secondary Bjerknes force obtained with matching pressures shows only weak dependence on the shear modulus. For the pressure amplitudes investigated, equilibrium distances can be found between two bubbles when the equilibrium radius of one of the bubbles is in a narrow range around 2μm. The equilibrium distance decreases when the shear modulus is increased. A simple relation between the two quantities is established.

Keywords: Acoustic cavitation, secondary Bjerknes force, non-Newtonian fluids, numerical simulations

1. Introduction

The dynamics of cavitation and oscillating bubbles in non-Newtonian fluids has been investigated for several decades (see e.g., Brujan [7], Gaudron et al. [15], Warnez and Johnsen [41] and references therein). A main impetus comes from biomedical applications[28, 25, 47], but applications are also found in other industries such as casting, welding, and galvanizing [12], where the non-Newtonian properties of molten metals are involved. Past research has looked into viscoelastic fluids that can be described by Kelvin-Voigt models [43, 15, 41] and Maxwell models [13, 39, 6, 2, 22, 14, 17, 41]. Numerical simulations based on compressible models find that generally elasticity tends to reduce the amplitude of the oscillation

*To whom correspondence should be addressed.
Email address: yili@sheffield.ac.uk. (Yi Li)

and increase the transient cavitation threshold. Nevertheless, under certain circumstances, elasticity may increase the amplitude of oscillation drastically and lead to chaotic behaviors (see, e.g., [22]). Elasticity could also lead to phase differences in the oscillations [2], and compressibility effects should be accounted for properly when the oscillations are strong.

The research cited above is only concerned with a single bubble. Bubble clusters or clouds also often appear in medical applications. The shielding effects of bubble clusters in shock wave lithotripsy are investigated experimentally in [40]. Experiments on controlling cavitation bubble cloud in lithotripsy are conducted in [19]. The interaction between two or more bubbles in these settings, however, has not received much attention. When two bubbles are oscillating in a acoustically driven fluid, the two bubbles experience an inter-bubble force, the so-called secondary Bjerknes force [5]. One of the intriguing features of the force is that it may change from being attractive to being repulsive as the two bubbles migrate towards each other. As a result, the force is important for the formation of stable bubble clusters, such as the "bubble grapes" or "acoustic streamers" [27, 5, 32, 30, 25]. Ignoring the coupling between the two bubbles, Bjerknes [4] argues that the force is attractive (repulsive) when the two bubbles oscillate in (out of) phase (see also [8]). The dependence on the inter-bubble distance is explained qualitatively by linear or weakly nonlinear theories [45, 9]. Subsequent research has looked into the effects of multiple scattering, nonlinearity, compressibility, shape oscillations, the coupling with the translation of the bubbles, and dual-frequency driving [36, 37, 11, 31, 3, 16, 35, 44, 21, 46]. Suggestions have been made to use the force to manipulate bubbles as carriers of micro-devices [18, 24, 1].

In a recent paper by Liu et al. [29], the secondary Bjerknes force between two bubbles encapsulated in viscoelastic films while oscillating in a Newtonian fluid is investigated. However, to the best of our knowledge, no similar research has been reported when the fluid itself is non-Newtonian. The focus of this paper is on the interactions, and specifically the second Bjerknes force, between two bubbles oscillating in a nonlinear Kelvin-Voigt (KV) fluid. For this fluid, a clean closed algebraic expression for the elastic stress term has been derived in Gaudron et al. [15], which significantly simplifies the analysis and has partly motivated our choice. For Newtonian fluids, the governing equations for a system of two bubbles are already available. For non-Newtonian fluids, it is necessary to re-examine some of the assumptions and derive the governing equations. Meanwhile, a more accurate model is needed to take into account the time-delay effect in the coupling between the two bubbles. These developments are presented in Section 2. The definition of the secondary Bjerknes force is reviewed in Section 3. In Section 4, the parameters characterizing the interaction of the two bubbles, such as the secondary Bjerknes force and the equilibrium distances, are calculated numerically. The results are compared with those in Newtonian fluids to elucidate the effects of the elasticity. The conclusions are summarized in section 5.

2. The governing equations

The bubbles are driven by a harmonic uniform pressure with angular frequency ω:

$$p_\infty(t) = p_0 - p_a \sin(\omega t) \tag{1}$$

where p_0 is the ambient pressure and p_a is the amplitude of the ultrasonic pressure. Cases with large p_a will be considered, where the bubbles experience rapid expansion (the so-called

transient cavitation) followed by violent collapse. Therefore, the compressibility effects will be taken into account. The bubbles are assumed to be spherical during the oscillations. For the parameters considered in this investigation, the deviation from this assumption is negligible (see Appendix A for a brief discussion).

Given these assumptions, the oscillation of a single bubble is described by the Keller-Miksis model [23, 43, 15]. The model is accurate up to $O(M)$, where $M \sim c_\infty^{-1}$ is the Mach number with c_∞ being the speed of sound in the unperturbed fluid. The model can be written as:

$$2\rho(1-c_\infty^{-1}\dot{R})R\ddot{R}+\rho(3-c_\infty^{-1}\dot{R})\dot{R}^2=2(1+c_\infty^{-1}\dot{R})(p_w-p_\infty)+2c_\infty^{-1}R(\dot{p}_w-\dot{p}_\infty), \quad (2)$$

where $R(t)$ is the radius of the bubble, ρ is the density of the fluid, and p_w is the pressure on the outer interface of the bubble. p_w has the following expression:

$$p_w=\left(p_0+\frac{2\sigma}{R_E}\right)\left(\frac{R_E}{R}\right)^{3k}-\frac{2\sigma}{R}-V(t), \quad (3)$$

in which σ denotes the surface tension, R_E is the equilibrium radius of the bubble, k is the polytropic exponent, and $V(t)$ is given by [15]

$$V(t)=\frac{4\rho\nu\dot{R}}{R}+\frac{\eta}{2}\left(5-4\frac{R_\circ}{R}-\frac{R_\circ^4}{R^4}\right), \quad (4)$$

where ν is the kinematic viscosity of the liquid, η is the shear modulus due to the elasticity, and $R_\circ$ is the initial radius of the bubble. $R_\circ$ is assumed to be the same as R_E in this paper. The expression for $V(t)$ in a Newtonian fluid is obtained when $\eta = 0$.

Note that, although the Keller-Miksis model was originally proposed for bubbles in Newtonian fluids, Brujan [6] and Yang and Church [43] have proven that the equation is still valid for various non-Newtonian fluids as long as the correct expression of $V(t)$ is used. Their argument can be used to show that the model is also valid for the KV fluid being investigated in this paper.

For a coupled two-bubble system with $R_1(t)$ and $R_2(t)$ as the radii of the two bubbles, Mettin et al. [31] introduces the coupling term

$$p_{ij}(t)=\frac{\rho}{D}\frac{dR_j^2\dot{R}_j}{dt}, \quad (i,j=1,2,i\neq j) \quad (5)$$

to model the interaction between the two bubbles, where D is the distance between the bubbles. Substituting Eq. 5 into Eq. 2, they obtain the following equation for $R_i(t)$:

$$\begin{aligned}2\rho(1-c_\infty^{-1}\dot{R}_i)R_i\ddot{R}_i+\rho(3-c_\infty^{-1}\dot{R}_i)\dot{R}_i^2=&\,2(1+c_\infty^{-1}\dot{R}_i)(p_{wi}-p_\infty)+2c_\infty^{-1}R_i(\dot{p}_{wi}-\dot{p}_\infty)\\&-2\rho D^{-1}(2R_{3-i}\dot{R}_{3-i}^2+R_{3-i}^2\ddot{R}_{3-i}),\end{aligned} \quad (6)$$

where p_{w_i} has the same expression as p_w except that R and R_E are replaced by R_i and R_{Ei}, respectively.

To generalize the above model to the KV fluids, two questions need to be addressed. Firstly, the validity of the coupling term p_{ij} given in Eq. 5 needs to be established for

the KV fluids. This is done in Appendix B. Secondly, as noted in Mettin et al. [31], Eq. 6 has omitted the time delay effect due to the finite propagation speed of pressure waves in compressible fluids. In a system of weakly oscillating bubbles, Doinikov et al. [10] incorporated the effect into the linearized equations, and improved the prediction in pressure fluctuations. However, for strong oscillations, the effect has not been considered.

In a compressible fluid, the pressure wave travels with a finite speed c_∞, so that the time for the pressure to propagate from one bubble to the other is D/c_∞. Thus, the pressure on bubble i should be $p_{ij}(t - D/c_\infty)$ where $p_{ij}(t)$ is given by Eq. (5) (see, e.g., [20, 10]). For bubble i, p_{ij} represents a change in the far field pressure. Therefore, to account for the coupling, the far field pressure $p_\infty(t)$ in the equation for bubble i is replaced by

$$p_\infty(t) + p_{ij}(t - D/c_\infty) \approx p_\infty(t) + p_{ij}(t) - Dc_\infty^{-1}\dot{p}_{ij}. \tag{7}$$

The right hand side of the above equation is an $O(M)$ approximation for the pressure on the left hand side. The approximation will be adopted since the Keller-Miksis model is accurate only up to $O(M)$ anyway. Using the RHS of Eq. (7) to replace p_∞ in Eq. (2), one obtains

$$\begin{aligned} 2\rho(1 - c_\infty^{-1}\dot{R}_i)R_i\ddot{R}_i + \rho(3 - c_\infty^{-1}\dot{R}_i)\dot{R}_i^2 = {} & 2(1 + c_\infty^{-1}\dot{R}_i)(p_{wi} - p_\infty) - 2(1 + c_\infty^{-1}\dot{R}_i)p_{ij} \\ & + 2c_\infty^{-1}R_i(\dot{p}_{wi} - \dot{p}_\infty) + 2c_\infty^{-1}(D - R_i)\dot{p}_{ij}. \end{aligned} \tag{8}$$

Note that some $O(M^2)$ terms arise in the substitution. These terms have been omitted, including the terms involving d^2p_{ij}/dt^2.

Finally, $\dot{p}_{ij}$ is removed from the above equation by substituting Eq. (5) into Eq. (8). The substitution leads to $\dddot{R}_j(t)$, the third order derivative of $R_j(t)$. As noted in [38], it can be evaluated from $\ddot{R}_j$ with $\dot{R}_j$ given by the Rayleigh-Plesset equation (see, e.g., [5]). As a result, the final model equation can be written as

$$\begin{aligned} & 2\rho(1 - c_\infty^{-1}\dot{R}_i)R_i\ddot{R}_i + 2\rho[D^{-1}(1 + c_\infty^{-1}\dot{R}_i)R_{3-i} + c_\infty^{-1}(D^{-1}R_i - 1)\dot{R}_{3-i}]R_{3-i}\ddot{R}_{3-i} \\ & + \rho(3 - c_\infty^{-1}\dot{R}_i)\dot{R}_i^2 + \rho[4D^{-1}(1 + c_\infty^{-1}\dot{R}_i)R_{3-i} + c_\infty^{-1}(D^{-1}R_i - 1)\dot{R}_{3-i}]\dot{R}_{3-i}^2 \\ = {} & 2(1 + c_\infty^{-1}\dot{R}_i)(p_{wi} - p_\infty) - 2c_\infty^{-1}(D^{-1}R_i - 1)\dot{R}_{3-i}(p_{w(3-i)} - p_\infty) \\ & + 2c_\infty^{-1}R_i(\dot{p}_{wi} - \dot{p}_\infty) - 2c_\infty^{-1}(D^{-1}R_i - 1)R_{3-i}(\dot{p}_{w(3-i)} - \dot{p}_\infty). \end{aligned} \tag{9}$$

Eq. (9) contains additional $O(M)$ terms not present in the previous model (i.e., Eq. (6)). These terms represent the time-delay effects. The equation applies to both Newtonian fluids and KV fluids with appropriate p_{wi}. Eq. (9) is the model developed in this paper; it will be compared with the previous models later in this paper.

3. The secondary Bjerknes force

Let F_{ij} denote the secondary Bjerknes force on bubble i induced by bubble j, where $i, j = 1, 2$ and $i \neq j$. By definition, F_{ij} is the time-averaged pressure force on bubble i generated by the oscillations of bubble j. For the moment, we neglect the time delay effects. F_{ij} can be written as (see, e.g., [8]):

$$F_{ij} = \left\langle V_i \left.\frac{\partial p_j}{\partial r}\right|_{r=D} \right\rangle = -\frac{\rho}{D^2}\left\langle V_i \frac{dR_j^2\dot{R}_j}{dt} \right\rangle = \frac{\rho}{4\pi D^2}\langle \dot{V}_i\dot{V}_j\rangle, \tag{10}$$

where V_i is the volume of bubble i and r in the above equation is the radial distance from the center of bubble j. The pointed brackets represent averaging over a period of the driving pressure. Note that, defined this way, the force is positive when it is attractive. Also, F_{ij} is symmetric, i.e., $F_{ij} = F_{ji}$. In terms of F_{ij}, the so-called secondary Bjerknes force factor f_{ij} (see, e.g., [31]) is defined as $f_{ij} \equiv \rho\langle \dot{V}_i \dot{V}_j \rangle / 4\pi \equiv D^2 F_{ij}$.

If the time delay is considered, the pressure gradient used in Eq. (10) should be evaluated at the retarded time $t - D/c_\infty$ (c.f. Section 2). Using Taylor expansion up to $O(M)$, one can show that the expression for the force should be modified to $F_{ij} + F^C_{ij}$ where the correction term F^C_{ij} reads

$$F^C_{ij} = -\frac{\rho}{4\pi D c_\infty} \langle \dot{V}_i \ddot{V}_j \rangle. \tag{11}$$

F^C_{ij} is anti-symmetrical with respect to the indices, i.e., $F^C_{ij} = -F^C_{ji}$, since we have $\langle \dot{V}_i \ddot{V}_j \rangle = -\langle \ddot{V}_i \dot{V}_j \rangle$. As a consequence, the two forces (i.e., F^C_{ij} and F^C_{ji}) point in the same direction. Under their effects, the two bubbles would tend to translate along the line joining the centers of the bubbles. In terms of the interaction between the two bubbles, this contribution represents a higher order effect, hence is neglected in current investigation.

4. Numerical results and discussions

We focus on strong oscillations with pressure amplitudes p_a above the transient cavitation threshold [31]. The equations are solved numerically. Results for a Newtonian fluid are computed to compare with those in the Kelvin-Voigt fluids. In order to validate our results, same parameters as those in Mettin et al. [31] have been used in the majority of cases, and water is chosen to represent the Newtonian fluid. The angular frequency ω of the driving pressure is chosen as $\omega = 2\pi f$ with $f = 2 \times 10^4\ s^{-1}$, so the period T is $5 \times 10^{-5} s$. The ambient pressure $p_0 \equiv p_{\rm atm} = 1.013 \times 10^5$Pa. The pressure amplitude is $p_a = 1.32 p_{\rm atm}$. The polytropic exponent is set at $k = 1.4$. Density $\rho = 998\ {\rm kg\,m^{-3}}$, surface tension coefficient $\sigma = 0.0725\ {\rm Nm^{-1}}$, speed of sound $c_\infty = 1500{\rm m\,s^{-1}}$, and kinematic viscosity $\nu = 1.002 \times 10^{-6}$ ${\rm m^2 s^{-1}}$. In medical applications, these parameters have been used in, e.g., intracorporeal lithotripsy [33]. In a few cases considered below, different p_a and f is also used to examine the universality of the results.

The bubbles are assumed to be in equilibrium initially. Therefore, the initial radii are given by the equilibrium radii R_{E1} and R_{E2}. Only bubbles with equilibrium radii at the order of several microns are considered since these are the typical sizes in medical applications (e.g. shock wave lithotripsy). Solutions for various combinations of (R_{E1}, R_{E2}) in this range are calculated. The Kelvin-Voigt fluid is a common model for soft tissues. Therefore the value for η is chosen from the data for soft tissues. According to Wells and Liang [42], the shear modulus for soft tissues can range from 1KPa to 100KPa in medical applications. Values up to 30KPa are examined in this paper. These values correspond to, for example, breast, kidney and liver tissues under various medical conditions.

4.1. The effects of time delay in Newtonian fluids

The model without time delay (given in Eq. (6)) is called the coupled Keller-Miksis model, CKM for short. The model with time delay (given in Eq. (9)) is called the coupled Keller-Miksis model with time delay, and is referred to as CKMTD in what follows. The

predictions in the Newtonian fluid made by the CKM and CKMTD models are compared in this section.

4.1.1. The secondary Bjerknes force

The general features are displayed in Fig. 1, where the radii of two pairs of bubbles are plotted. For better visibility, Results for bubble 2 are shown in Fig. 1a, and those for bubble 1 in Fig. 1b. The bubbles experience strong transient cavitation followed by a series of rebounds. Differences in the two models are observed in the rebound phase, which is more visible in Fig. 1b and the inset therein. The new model predicts stronger rebounds for the smaller bubble in each pair. The maximum radii $R_{\max}$ calculated by the two models also show some small differences. The differences are bigger for bubble with $R_{E2} = 10\mu$m, which suggests that they may increase with the size of the bubble.

The difference in the rebound phase has significant impact on the secondary Bjerknes force. Shown in Fig. 2 is the contour plot of the secondary Bjerknes force factor f_{12} (see the definition below Eq. (10)). As the plot is symmetric with respect to R_{E1} and R_{E2}, only half of the domain needs to be shown for each model. The main difference is observed for $R_{E1} \lesssim 2\mu$m and $R_{E2} \gtrsim 2\mu$m (or the other way around). In this range, the CKM model predicts positive f_{12}, which is a conclusion also reached in [31]. However, the CKMTD model predicts negative f_{12}. Quantitative difference is shown in Fig. 3 for two R_{E1} values. As the value of f_{12} spans several orders of magnitude for R_{E2} between 0 and 2μm, this range is shown separately in two insets. The top-right inset corroborates the aforementioned observation that f_{12} predicted by the two models has different signs for $R_{E2} \lesssim 1.8\mu$m. It also shows that the difference in f_{12} is larger for larger R_{E1}. There is a sharp drop in f_{12} between $R_{E2} = 1.8$ and 2μm. This is shown in the bottom-left inset (Note that the y-limits for the two insets are different).

A partially averaged secondary Bjerknes force $f_{12}^a(t)$ $(0 \le t \le T)$ is considered next, where

$$f_{12}^a(t) = \frac{1}{t}\int_0^t \frac{\rho \dot{V}_1 \dot{V}_2}{4\pi} dt. \tag{12}$$

$f_{12}^a(t)$ as a function of t can reveal the contributions to f_{12} from different phases of the oscillation, and, by definition, $f_{12} = f_{12}^a(T)$. $f_{12}^a(t)$ is shown in Fig. 4 for selected radii. $R_2(t)$ is also plotted to highlight the incipience of the rebound phase. The results for $f_{12}^a(t)$ from the two models start to diverge only when the bubbles approach the rebound phase. This verifies that the difference in f_{12} does come from the rebound phase.

Experimentally, stable clusters are observed even when the bubbles appear to oscillate in phase, seemingly contradicting the theoretical prediction that they should be attracted to each other (see, e.g., [30]). Our results provide a possible explanation. Although the bubbles are in phase in the expansion phase, our results show that they may be out of phase in the rebound stage (which is not always experimentally observable). This thus leads to a repulsive secondary Bjerknes force, hence stable clusters. The new model predicts that there is a wider range of bubble radii where bubbles repel each other.

4.1.2. The equilibrium distance

For given (R_{E1}, R_{E2}), f_{12} is a function of the inter-bubble distance D. The equilibrium distance D_E is defined as the distance D where $f_{12} = 0$ and $f_{12} > 0$ for $D > D_E$. At

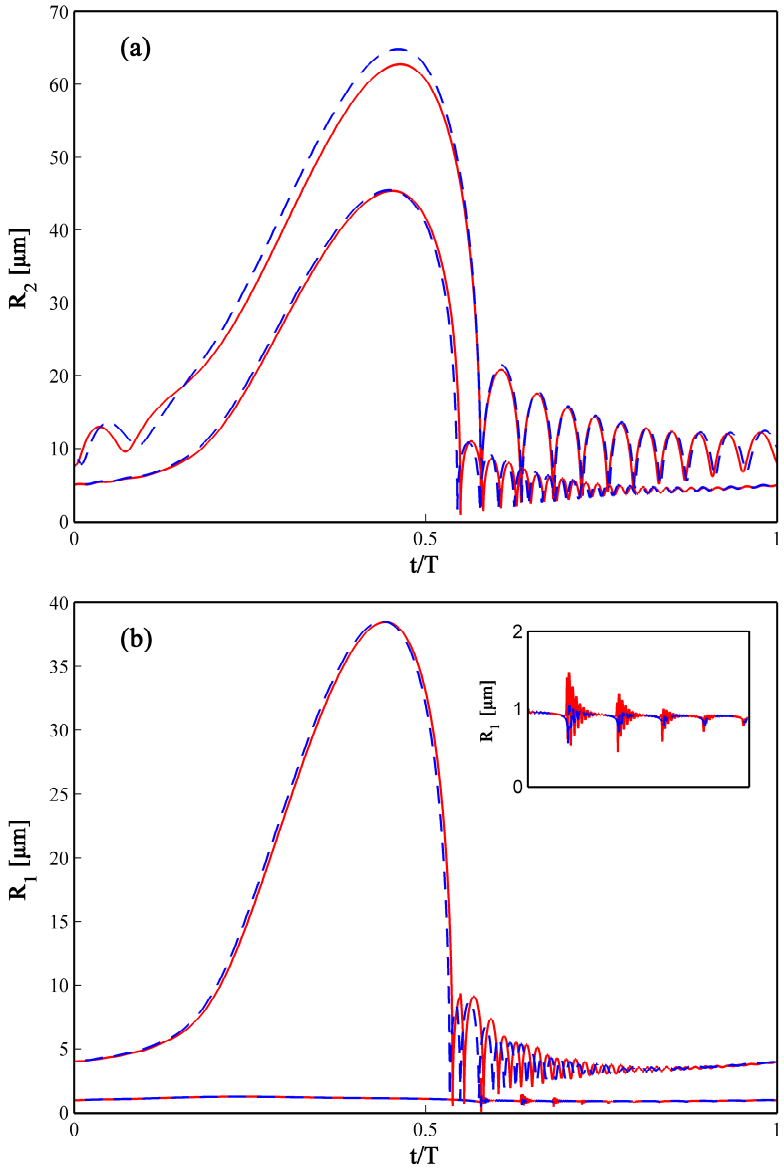

Figure 1: The radii of the bubbles $R_1(t)$ and $R_2(t)$, with $(R_{E1}, R_{E2}) = (1\mu\text{m}, 10\mu\text{m})$ (Case 1) and $(4\mu\text{m}, 5\mu\text{m})$ (Case 2). $p_a = 1.32 p_{\text{atm}}$. $f = 20$KHz. $D = 100\mu$m. (a): Results for $R_2(t)$. The top group: Case 1. Solid line: CKMTD; dashed line: CKM. The bottom group: Case 2. Solid line: CKMTD; dashed line: CKM. (b) Results for $R_1(t)$. The top group: Case 2. Solid line: CKMTD; dashed line: CKM. The bottom group and the inset: Case 1. Solid line: CKMTD; dashed line: CKM.

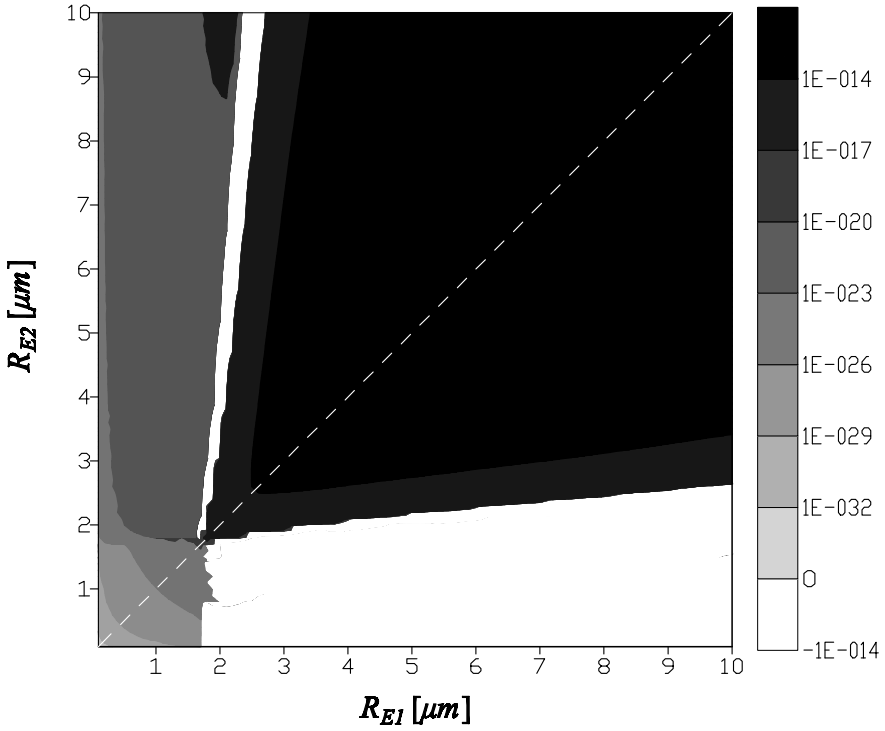

Figure 2: The secondary Bjerknes force factor f_{12} as a function of R_{Ei} $(i = 1, 2)$. The upper half: CKM; the lower half: CKMTD. $p_a = 1.32 p_{\rm atm}$. $f = 20$KHz. $D = 100\mu$m.

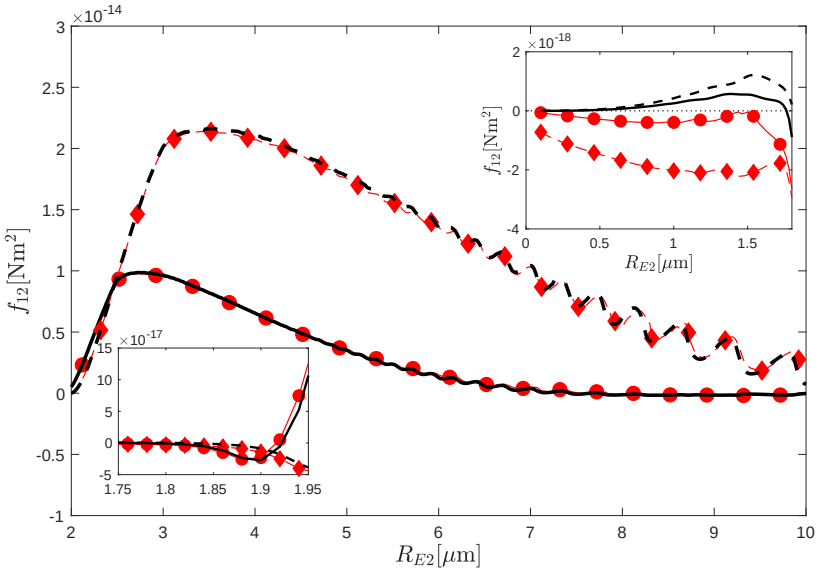

Figure 3: The secondary Bjerknes force factor f_{12} as a function of R_{E2}. Lines: CKM model. Solid line: $R_{E1} = 2.5\mu$m; dashed lines: $R_{E1} = 3\mu$m. Symbols: CKMTD model. Circles: $R_{E1} = 2.5\mu$m; diamonds: $R_{E1} = 3\mu$m. Top-right inset: $0 \le R_{E2} \le 1.8\mu$m; bottom-left inset: $1.75 \le R_{E2} \le 1.95\mu$m. $p_a = 1.32 p_{\rm atm}$. $f = 20$KHz. $D = 100\mu$m.

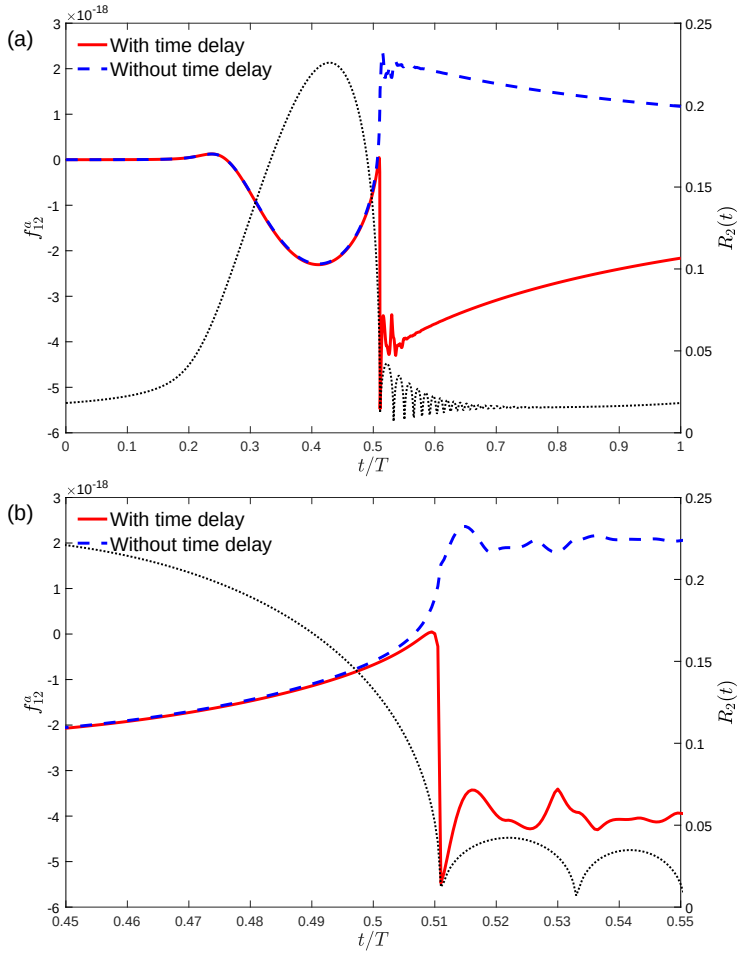

Figure 4: (a) $f_{12}^a(t)$ for $(R_{E1}, R_{E2}) = (3, 1.5)\mu$m, $p_a = 1.32 p_{\rm atm}$, and $D = 100\mu$m. Right y-axis and the dotted line: $R_2(t)$ from the CKMTD model. (b): A zoom-in around the beginning of the rebound phase.

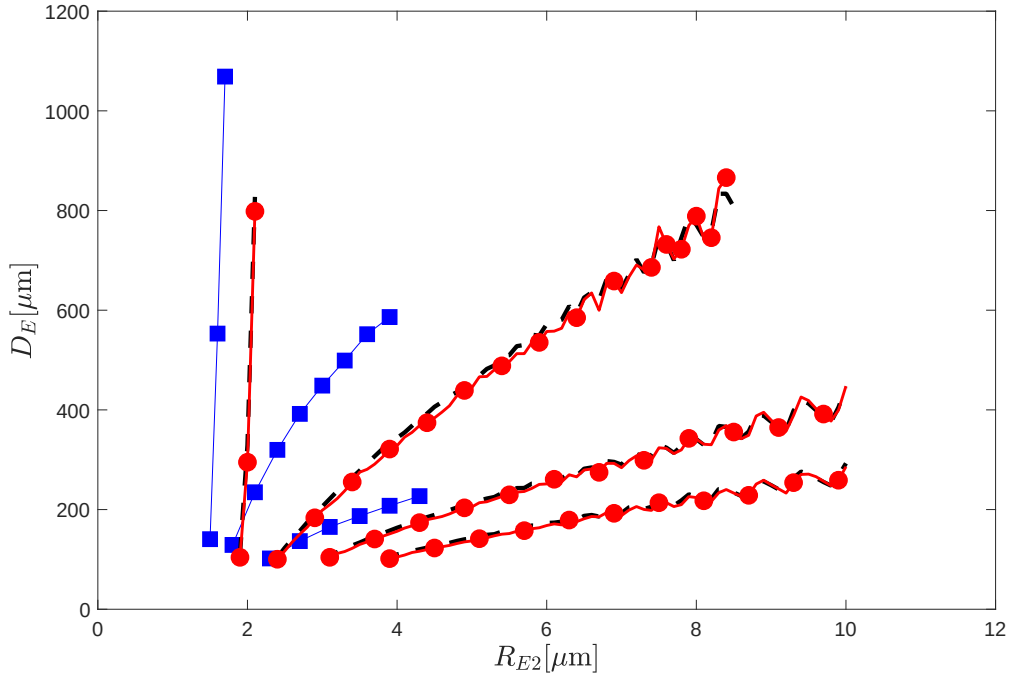

Figure 5: Equilibrium distance D_E as a function of R_{E2}. Dashed lines: CKM model; solid lines with circles: CKMTD model. Both with $p_a = 1.32p_{\mathrm{atm}}$. The four groups (from left to right) correspond to $R_{E1} = 1.8, 1.9, 2, 2.1\mu$m. Squares: CKMTD model with $p_a = 1.4p_{\mathrm{atm}}$. The three groups (from left to right) correspond to $R_{E1} = 1.45, 1.5, 1.6\mu$m.

this distance, the two bubbles experience no secondary Bjerknes force; if the bubbles drift apart, the force will become attractive and drive them towards each other, hence restoring their distance to D_E. D_E has been measured experimentally only recently for relatively large bubbles with small oscillations [44]. The experimental result was used to reveal some qualitative differences between experiments and theories. No data for D_E have been reported for the small bubbles investigated here. Therefore even the results from the old model would provide useful insights.

To calculate D_E for different bubbles, the radii R_{E1}'s for which equilibrium with some R_{E2}'s may exist are first identified with the help of Fig. 2. For each of these R_{E1}'s, every R_{E2} between 2 and 10μm is chosen, with a 0.1μm increment, to form a bubble pair. For each pair, f_{12} is calculated for different values of D, and a bisection search is used to find the roots of $f_{12} = 0$ and hence D_E. The search is stopped when the interval bracketing the root is narrowed down to 1μm. It is a time consuming calculation.

Fig. 5 plots D_E as a function of R_{E2} for four different R_{E1} for which D_E has been found to exist. The overall difference between the two models is small, with maximum relative difference being approximately 4%. No equilibrium distance is found for R_{E1} outside of the range of values shown in Fig. 5. For each R_{E1}, D_E increases with R_{E2} and the increasing rate strongly depends on R_{E1}. The squares in Fig. 5 show the results computed with the new model at $p_a = 1.4p_{\mathrm{atm}}$, to illustrate how the results depend on the pressure amplitude. D_E shows similar sensitive dependence on R_{E1} and R_{E2}. In both cases, equilibrium exists only for R_{E1} in a narrow range. For higher pressure amplitudes, the range for R_{E1} is shifted to smaller values, but only very slightly.

The result in Fig. 5 can qualitatively explain some behaviours of small bubble clusters [30]. Small clusters with diameters between 200μm and 500μm are often observed in 20KHz ultrasonic pressure fields with amplitude around $1.68p_{\rm atm}$ (see, e.g., page 22 in [30]). The radii of the bubbles are at the order of few microns. As stated by Mettin [30], it is unclear why the clusters are stable while the positions of the bubbles can change drastically within an oscillation cycle. Fig. 5 shows that D_E depends very sensitively on R_{E1} and R_{E2}, Therefore, the equilibrium distance can vary wildly with small changes in the equilibrium radii of the bubbles. In the small clusters, such a drastic change in the equilibrium distance between two bubbles may be triggered by rectified diffusion [5] or the perturbation from other bubbles, hence leading to the strong variations described in [30]. Fig. 5 shows that the high sensitivity is observed for different pressure amplitudes. Therefore the above explanation is expected to be qualitatively valid in general.

Though the two models produce similar D_E, the new model predicts larger repulsive secondary Bjernkes force, as shown in the insets of Fig. 3. Therefore, according to the new model, the equilibrium distance would be more stable than it is implied by the old model.

4.2. Results in the Kelvin-Voigt fluid

In this subsection, only the new model is applied to investigate the secondary Bjerknes force in Kelvin-Voigt fluids with different shear modulus η.

4.2.1. General features

The general features of the results are first reported. Fig. 6a shows radius $R_1(t)$ for a pair of bubbles with $(R_{E1}, R_{E2}) = (3, 4)\mu$m for several values of η. The top curve corresponds to the Newtonian fluid. As η is increased, the maximum radius is reduced and the transient cavitation phase is shortened. For $\eta = 10$KPa, transient cavitation is already almost suppressed. The result reproduces the known effects of elasticity [15], i.e., the elastic stress reduces the amplitude of the oscillations. The secondary Bjerknes force factor f_{12} is, as expected, also reduced by elasticity, as shown in Fig. 6b. Even for this moderate value of η, f_{12} can be several orders of magnitude smaller than its values in the Newtonian fluid.

4.2.2. The matching pressure

To make the comparison in different KV fluids more informative, the parameters in each case should be chosen in such a way that different cases are comparable. Instead of simply changing η while keeping other parameters the same for different cases, the method adopted here is to compare *the cases with same level of transient cavitation*. From a practical point of view, this is a more useful comparison.

For this purpose, the maximum radius $R_{\rm max}$ for a single oscillating bubble is used to measure the strength of the transient cavitation, and a matching pressure, denoted by p_m, is defined. Let p_a^N be the value of p_a used to drive the bubble in a Newtonian fluid, and $R_{\rm max}$ be the maximum radius achieved by the bubble. Considering the oscillation of a bubble in a KV fluid, p_m is defined as the value of p_a needed to drive the bubble so that its maximum radius is also $R_{\rm max}$. p_m is a function of p_a^N and η, so one may write $p_m(p_a^N, \eta)$. For a given p_a^N, two cases with different η's are comparable when the pressure amplitudes p_a's are given by $p_m(p_a^N, \eta)$. By itself, p_m also provides useful information about the ultrasonic power needed in different KV fluids to maintain the same level of transient cavitation.

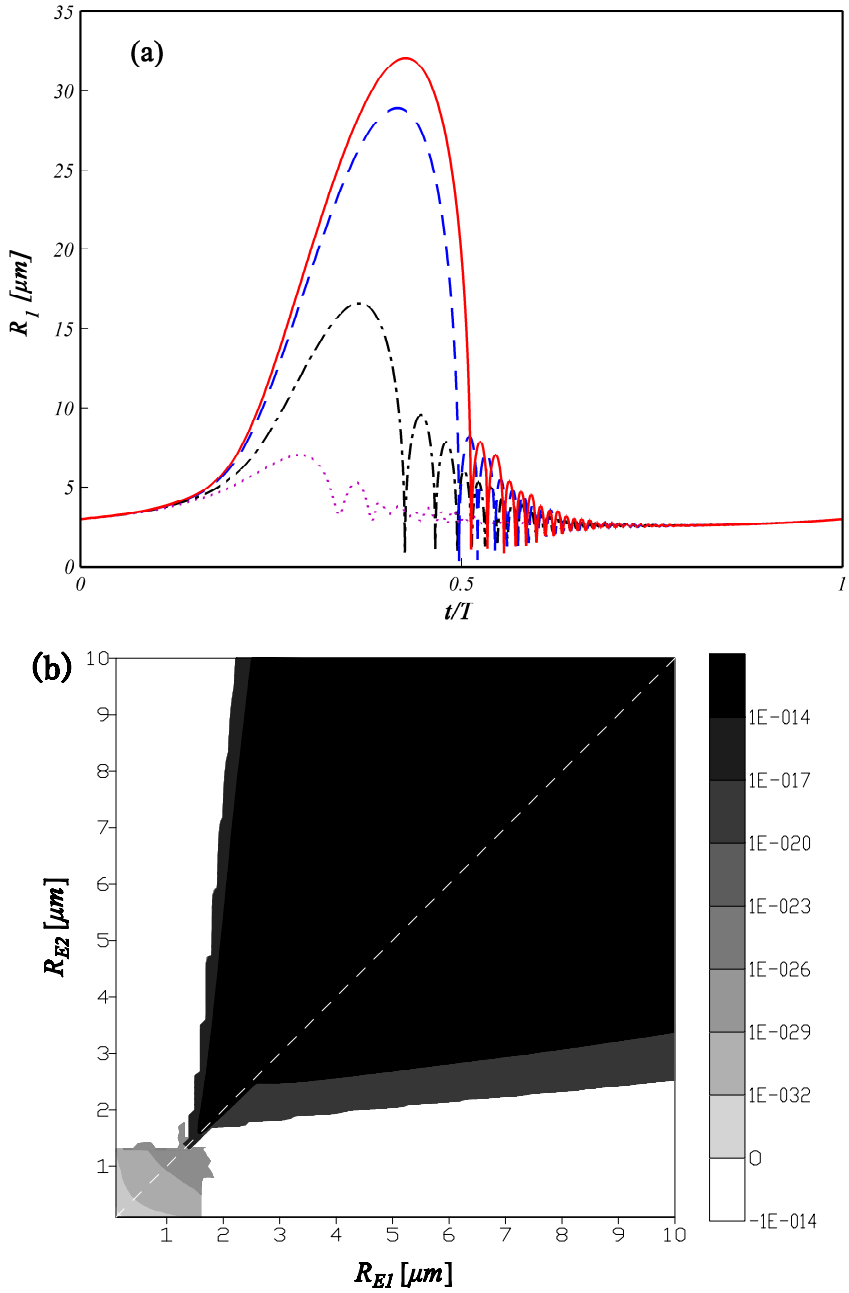

Figure 6: (a) The radius $R_1(t)$ for bubbles with $(R_{E1}, R_{E2}) = (3, 4)\mu$m, calculated with $D = 0.1$mm and $p_a = 1.32 p_{\rm atm}$. From the top to bottom, $\eta = 0, 1, 5, 10$KPa. (b) The force factor f_{12} for the KV fluid (lower half) with $\eta = 5$KPa and the Newtonian fluid (upper half). $p_a = 1.42 p_{\rm atm}$. $f = 20$KHz. $D = 100\mu$m.

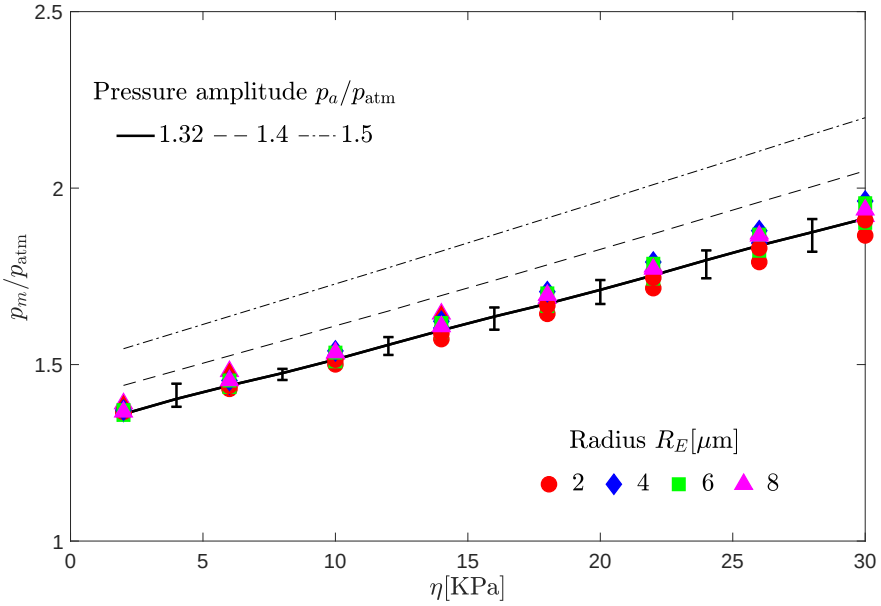

Figure 7: The matching pressure p_m as a function of η. Symbols are calculated with $p_a^N = 1.32p_{\rm atm}$, $f = 20$KHz and 30KHz (shown with same symbols). Solid line: averaged p_m. Error bars show the variations between the cases. Dashed and dash-dotted lines: the matching pressure for $p_a^N = 1.4$ and $1.5p_{\rm atm}$ with $f = 20$KHz and $R_E = 2\mu$m.

Fig. 7 shows p_m obtained numerically for $R_E = 2, 4, 6, 8\mu$m and $p_a^N = 1.32p_{\rm atm}$. In each case, results for two frequencies $f = 20$KHz and 30KHz are computed. Results with $p_a^N = 1.4$ and $1.5p_{\rm atm}$ are also calculated for $R_E = 2$ and $f = 20$KHz to illustrate the dependence of p_m on p_a^N. It is observed that p_m increases with η essentially linearly. For given p_a^N and η, the variations with R_E and f are smaller than 10%. The slopes of the lines only change very slightly with p_a^N. Therefore, for a given p_a^N, the averaged p_m between different cases provide a good approximation to the matching pressure for different R_E or f. The averaged p_m is shown with the solid line. The curve can be approximated by the following linear function:

$$\frac{p_m}{p_{\rm atm}} = \frac{p_a^N}{p_{\rm atm}} + 0.0214\eta, \tag{13}$$

where η is given in KPa. Eq. 13 can be used to estimate the pressure amplitude needed to produce same transient cavitation in different KV fluids.

4.2.3. The secondary Bjerknes force and the equilibrium distance

The secondary Bjerknes force factor f_{12} for different η is then calculated with the corresponding matching pressure $p_m(p_a^N, \eta)$ for $p_a^N = 1.32p_{\rm atm}$. Six cases are computed where $(R_{E1}, R_{E2}) = (2, 4), (2, 6), (2, 8), (4, 6), (4, 8)$ and $(6, 8)\mu$m, respectively. These cases provide a full picture of the force for bubbles with radii of a few microns.

Fig. 8 plots f_{12} for different η and radii between 4 and 8μm. The results segregate in two groups according to the value of R_{E1}. The average over all cases in each group is shown with the solid lines. Computation shows that the deviation from the average is within 15% in both groups. Therefore, the variation with η is significantly reduced using the matching

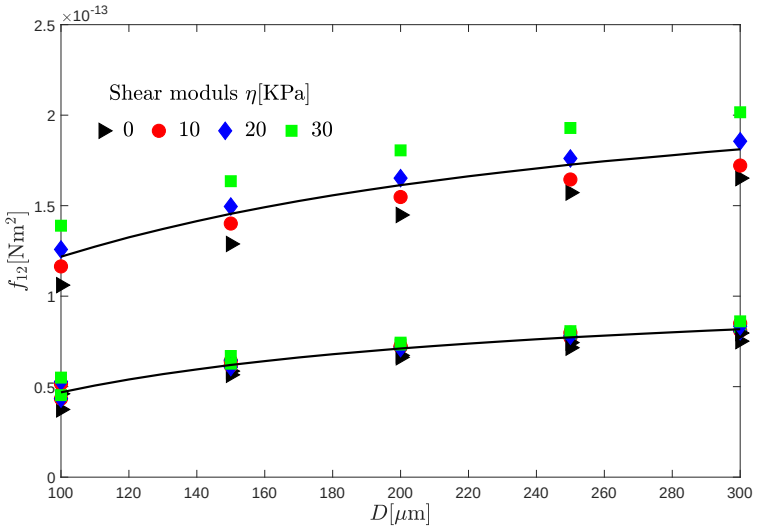

Figure 8: f_{12} versus D. Top group: $(R_{E1}, R_{E2}) = (6, 8)\mu$m. Bottom group: $(4, 6)$ and $(4, 8)\mu$m. Solid lines: the average in each group. Calculated with matching pressure for $p_a^N = 1.32 p_{\rm atm}$, $f = 20$KHz.

pressure, which shows that it is an effective way to correlate the data. Data shown in Fig. 8 are useful for the simulation of bubble clusters using particle methods (see, e.g., [32]).

For R_{E1} around 2μm, using the matching pressure also reduces the variations of the force with η. However, for radii in this range, the equilibrium distance D_E may exist. The variation of D_E with η may still be important even when the matching pressure is used. The situation is illustrated in Fig. 9 for $R_{E1} = 2\mu$m. The figures show that f_{12} increases with η, and as a consequence D_E decreases with η for all these bubble pairs.

The quantitative results for D_E with $\eta = 5$KPa is given in Fig. 10a. This relatively small η is chosen to show how D_E deviates from the value in the Newtonian fluid. The figure shows that the curves for slightly different R_{E1}'s can have very different slopes. For small R_{E1}, D_E increases with R_{E2} rapidly. Fig. 10b plots D_E for a wider range of η for selected radii. D_E is larger for larger bubbles, but in all cases it decreases with η. Note that, smaller D_E can still be found for some even larger η values. However, D_E smaller than 100μm is considered not realistic because the spherical bubble assumption used in the model becomes questionable when the distance between the bubbles is too small.

Let D_E^N be the value of D_E for the Newtonian fluid, given by the curves in Fig. 10b for $\eta = 0$. Fig. 10b suggests that D_E^N/D_E may have simple functional dependence on η. D_E^N/D_E is plotted in Fig. 11, which shows that the linear regression

$$\frac{D_E^N}{D_E} = a\eta + b \tag{14}$$

provides good approximation. The values for a and b found by least squares are given in the figure for each R_{E2}. The range of η in which $D_E \geq 100\mu$m is also given, which is the range in which the linear regression is valid.

Eq. 14 can be used to estimate the equilibrium distance between two bubbles hence the size of a bubble cluster in Kelvin-Voigt fluids. The observation that D_E decreases with η implies that stable bubble clusters in Kelvin-Voigt fluids may have smaller sizes, or may not

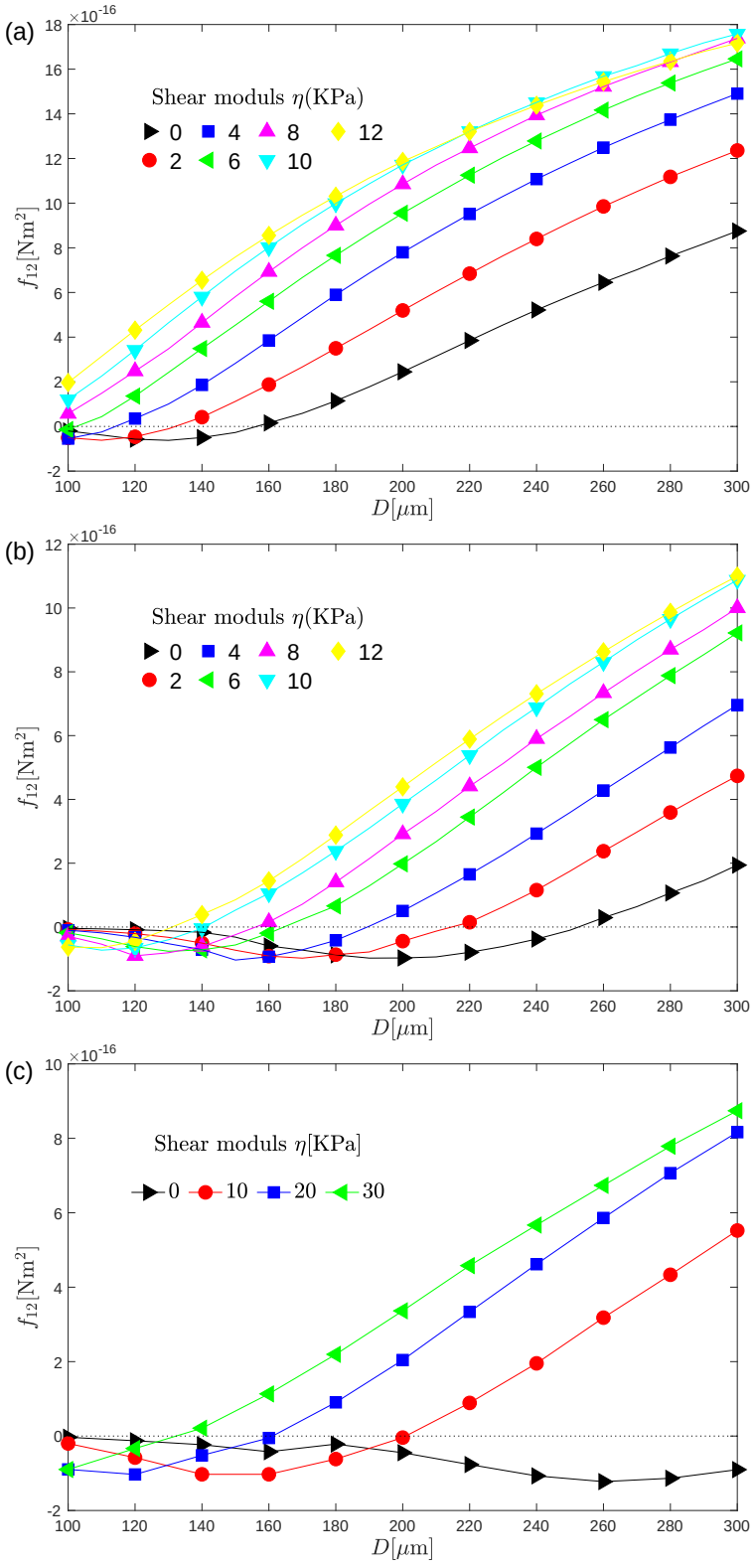

Figure 9: f_{12} versus D. Calculated with matching pressure for $p_a^N = 1.32 p_{\text{atm}}$, $f = 20$KHz. (a) $(R_{E1}, R_{E2}) = (2, 4)\mu$m. (b) $(R_{E1}, R_{E2}) = (2, 6)\mu$m. (c) $(R_{E1}, R_{E2}) = (2, 8)\mu$m.

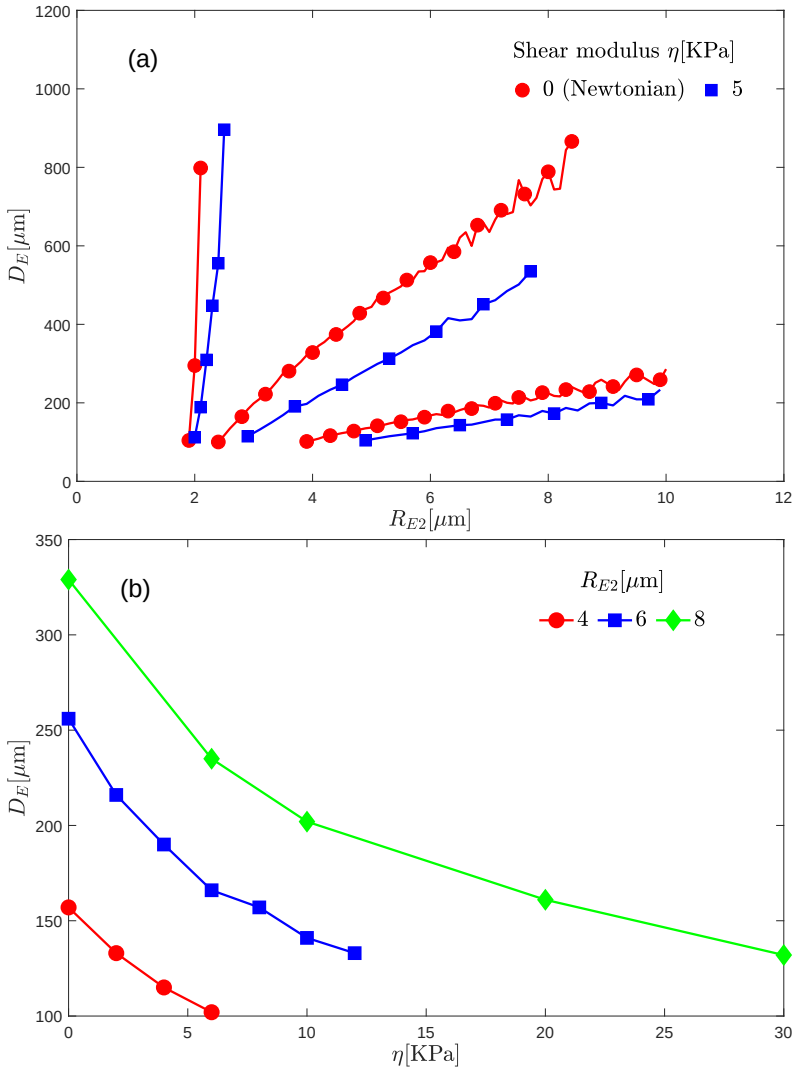

Figure 10: (a) The equilibrium distance D_E as a function of R_{E2} for $R_{E1} = 1.8, 1.9, 2.1\mu$m (from left to right). Circles: Newtonian fluid. Squares: KV fluid with $\eta = 5$KPa and matching pressure. $p_a^N = 1.32 p_{\mathrm{atm}}$. $f = 20$KHz. (b) The equilibrium distance D_E as a function for η, for $R_{E1} = 2\mu$m and $R_{E2} = 4, 6, 8\mu$m (bottom to top). $p_a^N = 1.32 p_{\mathrm{atm}}$. $f = 20$KHz.

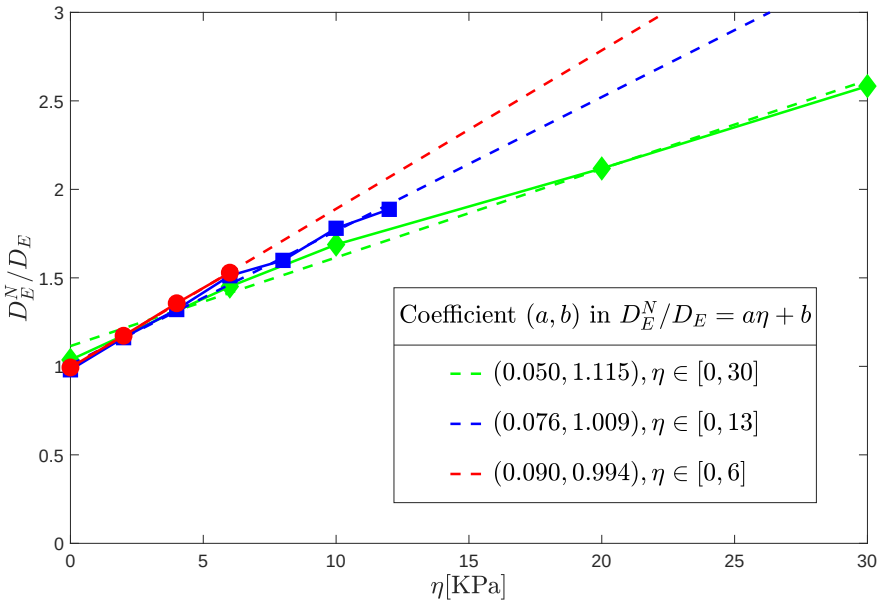

Figure 11: The linear regression for D_E^N/D_E where D_E^N is the equilibrium distance for the Newtonian fluid. η is given in KPa. Symbols are the same as in Fig. 10b.

be able to sustain, especially for higher η values. The implications on medical applications is worth further investigation.

5. Conclusions

A model taking into account the time-delay effect is derived and applied to study the interactions between two bubbles driven by harmonic ultrasonic pressure in a nonlinear Kelvin-Voigt (KV) fluid. The secondary Bjerknes force and the equilibrium distance between the bubbles are investigated. The matching pressure that produces same level of transient cavitation in different KV fluids is calculated, and is show to be effective in correlating the results in the KV fluid. The investigation is limited to the periodic transient cavitation regime for small bubbles with radii of a few microns. Several conclusions can be made from the analyses:

1. The time-delay effect leads to a new prediction that small bubbles are repelled by large bubbles. As a consequence, the chances to observe bubbles repelling each other are significantly higher than previously believed.
2. The rebound phase could have significant effects on the secondary Bjerknes force.
3. When the bubbles are driven by the matching pressure so that same level of transient cavitation is produced, the secondary Bjerknes force increases with the shear modulus of the fluid, whereas the equilibrium distance is inversely proportional to a linear function of the shear modulus.
4. The matching pressure shows only weak dependence on bubble radius and the frequency.
5. The equilibrium distance is very sensitive to the equilibrium radii of the bubbles.

The above observations have already offered new insights into some experimental observations reported in the literature. However, there are questions remained to be answered. The implications of the findings in medical applications need to be clarified. The current article does not cover all non-Newtonian fluid models. Important omissions include the Maxwell-type fluids or, more generally, the Oldroyd-B fluids. Further investigations are also needed to address problems where the bubbles do not remain spherical.

6. Acknowledgment

The authors gratefully acknowledge the support provided by the Guangdong provincial Science (Technology) Research Project (Project No. 2015A010105026) and the Guangzhou Science (Technology) Research Project (Project No. 201704030010).

Appendix A. The spherical bubble assumption

The deformation of the bubbles is negligible when the distance between the bubbles is not too small. However, a systematic investigation on the minimum distance has not been reported in the literature and is beyond the scope of this paper. Nevertheless, a reasonable estimate can be obtained by the Moore's formula for the deformation of a bubble rising with a given speed u in a quiescent Newtonian fluid. In this case, the spherical bubble becomes an ellipsoid, and the aspect ratio χ of the ellipsoid is given by the Moore's formula [34, 26]:

$$\chi = 1 + \frac{9}{64}\mathcal{W}, \tag{A.1}$$

where $\mathcal{W} \equiv 2\rho u^2 R/\sigma$ is the Weber number, with R being the average radius of the bubble. When this formula is applied to estimate the deformation of bubble 1 in the two bubbles, u should be the velocity at the location of bubble 1 induced by the oscillation of bubble 2. Using the simulation results for $R_{E1} = 6\mu$m, $R_{E2} = 8\mu$m, and $D = 100\mu$m, u is estimated to be 0.4ms^{-1}. This corresponds to the maximum velocity induced by bubble 2 when it collapses. R is estimated by the maximum radius of bubble 1, which is 44μm. $\mathcal{W}$ is thus approximately 0.2, giving $\chi \approx 1.03$. That is, there is only approximately 3% difference between the lengths of the axes of the ellipsoid. The difference is expected to be smaller for larger D. Therefore, for the bubbles simulated in this paper, $D = 100\mu$m is the minimum distance for which the deformation of the bubbles is negligible.

Appendix B. The coupling term for the nonlinear Kelvin-Voigt fluid

For a coupled two bubble system in a Kelvin-Voigt fluid, the coupling term similar to the one in Eq. (5) can be derived from the radial momentum equation, following the method in [31]. Considering the fluid motion around a single bubble, the radial velocity at a distance r from the centre of the bubble is given by $R^2\dot{R}/r^2$. Neglecting the viscous stress, the radial momentum equation becomes:

$$\frac{\partial p}{\partial r} = -\frac{\rho}{r^2}\frac{dR^2\dot{R}}{dt} + \frac{2\rho R^4\dot{R}^2}{r^5} + \eta\left(\frac{8}{3}\frac{r_\circ}{r^2} - \frac{10}{3}\frac{r}{r_\circ^2} + \frac{4}{3}\frac{r^4}{r_\circ^5} - \frac{2}{3}\frac{r_\circ^4}{r^5}\right), \tag{B.1}$$

where $r_\circ$ is the initial radial location of a material point whose current location is r. As noted in [15], assuming traceless stress tensor, one may obtain

$$r_\circ(r,t) = [r^3 - R(t)^3 + R_\circ^3]^{1/3}. \tag{B.2}$$

The last term on the RHS of Eq. B.1 is the contribution from the elasticity. Using Eq. (B.2) and expanding $r_\circ/r$ as a power series of $1/r$, Eq. B.1 becomes

$$\frac{\partial p}{\partial r} = -\frac{\rho}{r^2}\frac{dR^2\dot{R}}{dt} + \frac{2\rho R^4\dot{R}^2}{r^5} + \frac{2\eta}{3}\frac{(R_\circ^3 - R^3)^2}{r^7} + O(r^{-10}). \tag{B.3}$$

Therefore, the contribution from the elastic stress is $O(r^{-7})$. As in the models for Newtonian fluids, terms of $O(r^{-5})$ and smaller are neglected. Therefore, the pressure gradient is approximately given by the first term on the RHS. As a result, the coupling term in the Kelvin-Voigt fluid is the same as the one given in Eq. (5).

[1] Ahmed, D., Lu, M., Nourhani, A., Lammert, P. E., Stratton, Z., Muddana, H. S., Crespi, V. H., Huang, T. J., 2015. Selectively manipulable acoustic-powered microswimmers. Scientific Reports 5, 9744.

[2] Allen, J., Roy, R., 2000. Dynamics of gas bubbles in viscoelastic fluids. ii. nonlinear viscoelasticity. J. Acoust. Soc. Am. 108, 1640–1650.

[3] Barbat, T., Ashgriz, N., Liu, C.-S., 1999. Dynamics of two interacting bubbles in an acoustic field. J. Fluid Mech. 389, 137–168.

[4] Bjerknes, V. F. K., 1906. Fields of Force. Columbia University press, New York.

[5] Brennen, C. E., 1995. Cavitation and bubble dynamics. Oxford University Press.

[6] Brujan, E. A., 1999. A first-order model for bubble dynamics in a compressible viscoelastic liquid. J. Non-Newtonian Fluid Mech. 84, 83–103.

[7] Brujan, E. A., 2011. Cavitation in Non-Newtonian Fluids. Springer-Verlag Berlin Heidelberg.

[8] Crum, L. A., 1975. Bjerknes forces on bubbles in a stationary sound field. The Journal of the Acoustical Society of America 57, 1363.

[9] Doinikov, A. A., 1999. Effects of the second harmonic on the secondary bjerknes force. Phys. Rev. E 59, 3016–3021.

[10] Doinikov, A. A., Manasseh, R., Ooi, A., 2005. Time delays in coupled multibubble systems. The Journal of the Acoustical Society of America 117, 47.

[11] Doinikov, A. A., Zavtrak, S. T., 1995. On the mutual interaction of two gas bubbles in a sound field. Phys. Fluids 7, 1923.

[12] Eskin, G. I., Eskin, D. G., 2003. Production of natural and synthesized aluminum-based composite materials with the aid of ultrasonic (cavitation) treatment of the melt. Ultrasonic Sonochemistry 10, 297–301.

[13] Fogler, H. S., Goddard, J. D., 1970. Collapse of spherical cavities in viscoelastic fluids. Phys. Fluids 13, 1135.

[14] Foteinopoulou, K., Laso, M., 2010. Numerical simulation of bubble dynamcis in a phan-thien-tanner liquid: Non-linear shape and size oscillatory response under periodic pressure. Ultrasonics 50, 758–776.

[15] Gaudron, R., Warnez, M. T., Johnsen, E., 2015. Bubble dynamics in a viscoelastic medium with nonlinear elasticity. Journal of Fluid Mechanics 766, 54–75.

[16] Harkin, A., Kaper, T. J., Nadim, A., 2001. Coupled pulsation and translation of two gas bubbles in a liquid. J. Fluid Mech. 445, 377–411.

[17] Hua, C., Johnsen, E., 2013. Nonlinear oscillations following the rayleigh collapse of a gas bubble in a linear viscoelastic (tissue-like) medium. Phys. Fluids 25, 083101.

[18] Ida, M., 2009. Multibubble cavitation inception. Phys. Fluids 21, 113302.

[19] Ikeda, T., Yoshizawa, S., Tosaki, M., Allen, J. S., Takagi, S., Ohta, N., Kitamura, T., Matsumoto, Y., 2006. Cloud cavitation control for lithotripsy using high intensity focused ultrasound. Ultrasound in Med. & Biol, 32, 1383–1397.

[20] Ilinskii, Y. A., Zabolotskaya, E. A., 1992. Cooperative radiation and scattering of acoustic waves by gas bubbles in liquids. The journal of the Acoustical Society of America 92, 2837.

[21] Jiao, J., He, Y., Kentish, S. E., Ashokkumar, M., Manasseh, R., Lee, J., 2015. Experimental and theoretical analysis of secondary bjerknes forces between two bubbles in a standing wave. Ultrasonics 58, 35–42.

[22] Jimenez-Fernandez, J., Crespo, A., 2005. Bubble oscilation and inertial cavitation in viscoelastic fluids. Ultrasonics 43, 643–651.

[23] Keller, J. B., Miksis, M., 1980. Bubble oscillations of large amplitude. J. Acoust. Soc. Am. 68, 628–633.

[24] Lanoy, M., Derec, C., Tourin, A., Leroy, V., 2015. Manipulating bubbles with secondary bjerknes forces. Appl. Phys. Lett. 107, 214101.

[25] Lauterborn, W., Kurz, T., 2010. Physics of bubble oscillations. Rep. Prog. Phys. 73, 106501.

[26] Legendre, D., Zenit, R., Velez-Cordero, R., 2012. On the deformation of gas bubbles in liquids. Phys. Fluids 24, 043303.

[27] Leighton, T. G., 1994. The Acoustic Bubble. Academic Press, London.

[28] Lingeman, J. E., 1997. Extracorporeal shock wave lithotripsy: Development, instrument, and current status. Urol. Clin. North Am. 24, 195–211.

[29] Liu, Y., Sugiyama, K., Takagi, S., 2016. On the interaction of two encapsulated bubbles in an ultrasound field. J. Fluid Mech. 804, 58–89.

[30] Mettin, R., 2005. Bubble structures in acoustic cavitation. In: Doinikov, A. (Ed.), Bubble and Particle Dynamics in Acoustic Fields: Modern Trends and Applications. Kerala, India: Research Signpost, pp. 1–36.

[31] Mettin, R., Akhatov, I., Parlitz, U., Ohl, C. D., Lauterborn, W., 1997. Bjerknes forces between small cavitation bubbles in a strong acoustic field. Phys. Rev. E 56, 2925.

[32] Mettin, R., Luther, S., Ohl, C.-D., Lauterborn, W., 1999. Acoustic cavitation structures and simulations by a particle model. Ultrasonics Sonochemistry 6, 25–29.

[33] Miller, D., N.Smith, Bailey, M., Czarnota, G., Hynynen, K., Makin, I., of Ultrasound in Medicine Bioeffects Committee, A. I., 2012. Overview of therapeutic ultrasound applications and safety considerations. J. Ultrasound Med. 31, 623–634.

[34] Moore, D. W., 1959. The rise of a gas bubble in a viscous liquid. J. Fluid Mech. 6, 113.

[35] Pelekasis, N. A., Gaki, A., Doinikov, A., Tsamopoulos, J. A., 2004. Secondary bjerknes forces between two bubbles and the phenomenon of acoustic streamers. J. Fluid Mech. 500, 313–347.

[36] Pelekasis, N. A., Tsamopoulos, J. A., 1993. Bjerknes forces between two bubbles. part 1. response to a step change in pressure. J. Fluid Mech. 254, 467–499.

[37] Pelekasis, N. A., Tsamopoulos, J. A., 1993. Bjerknes forces between two bubbles. part 2. response to an oscillatory pressure field. J. Fluid Mech. 254, 501–527.

[38] Prosperetti, A., Lezzi, A., 1986. Bubble dynamics in a compressible liquid. part 1. first-order theory. J. Fluid Mech. 168, 457–478.

[39] Tanasawa, I., Yang, W.-J., 1970. Dynamic behavior of a gas bubble in viscoelastic liquids. Journal of Applied Physics 41, 4526.

[40] Wang, J.-C., Zhou, Y., 2015. Suppressing bubble shielding effect in shock wave lithotripsy by low intensity pulsed ultrasound. Ultrasonics 55, 65–74.

[41] Warnez, M. T., Johnsen, E., 2015. Numerical modelling of bubble dynamics in viscoelastic media with relaxation. Physics of Fluids 27, 063103.

[42] Wells, P. N. T., Liang, H.-D., 2011. Medical ultrasound: imaging of soft tissue strain and elasticity. J. R. Soc. Interface 8, 15211549.

[43] Yang, X., Church, C. C., 2005. A model for the dynamics of gas bubbles in soft tissues. J. Acoust. Soc. Am. 118, 3595–3606.

[44] Yoshida, K., Fujikawa, T., Watanabe, Y., 2011. Experimental investigation on reversal of secondary bjerknes force between two bubbles in ultrasonic standing wave. The Journal of the Acoustical Society of America 130, 135.

[45] Zabolotskaya, 1984. Interaction of gas bubbles in a sound field. Sov. Phys. Acousti. 30, 365.

[46] Zhang, Y., Zhang, Y., Li, S., 2016. The secondary bjerknes force between two gas bubbles under dual-frequency acoustic excitation. Ultrasonics Sonochemistry 29, 129–145.

[47] Zong, Y., Xu, S., Matula, T., Wan, M., 2015. Cavitation-enhanced mechanical effects and applications. In: Wan, M., Feng, Y., ter Haar, G. (Eds.), Cavitation in Biomedicine: Principles and Techniques. Springer, p. 207.